NANO · MICRO small
www.small-journal.com

Diffusion Coefficients of Coated Plasmonic Nanoparticles in Viscous Environment

*Isabelle Largillière, Dali Sullivan, and Michel Meunier**

The Stokes-Einstein relationship (SER) is not valid anymore in polymeric solutions for nanoparticles. It is thus important to characterize their diffusion properties to get a finer understanding of their behavior and to better tune their attributes for biomedical applications. The diffusion of gold and silver nanoparticles with citrate, hyaluronic acid, methyl-polyethylene glycol, and antibody-polyethylene glycol coatings is studied in hyaluronic-based viscous solutions. The diffusion coefficient D is estimated from the Brownian motion thanks to a cost-effective side-illumination device. It is determined that the nanoparticles (hydrodynamic radius r_h: 30–135 nm) diffuse up to 4–5 times faster than expected using the SER with a macroscopic viscosity from 1 to 30 mPa·s. It is shown that the adapted Huggins equation is a good model to describe the diffusion behavior of nanoparticles using an effective viscosity η_{eff} given by $ln\left(\frac{\eta_{eff}}{\eta_s}\right) = k\left(\frac{R_{eff}}{E}\right)^a$ where $R_{eff}^{-2} = r_h^{-2} + R_h^{-2}$ where E is the polymer correlation length, R_h the polymer hydrodynamic radius and η_s the solvent viscosity. The values of k and a are given and allow to obtain D with an error of 10–20%. The impact of chemical interactions on the model parameter values are also highlighted, especially due to electrostatic interactions between the polymer and the nanoparticles.

1. Introduction

Plasmonic nanoparticles (NPs) are useful in a large range of applications thanks to their unique optical characteristics. Their scattering and absorption properties are used in biomedicine applications, electronics, and the energy field.[1] The biomedical sphere leverages their surface chemistry properties for functionalization and specificity. It also relies on their biocompatibility in the case of gold NPs (AuNPs), or conversely, biocidal activity for silver NPs (AgNPs). Plasmonic NPs have great optical properties – scattering or absorption – for imaging use, sensor development, use as contrast agents, or therapeutic purposes.[1–3] However, biological fluids are complex, and NPs can have difficulties reaching the target area. That can be highly problematic for biomedical applications where specificity is essential. Some viscous environments such as lymphatic fluids, mucus, extracellular matrix, or vitreous, are responsible for reduced diffusion when compared to water.[4,5] Indeed, in addition to the viscosity, the interactions between NPs and structural proteins or glycosaminoglycans present in those fluids are expected to alter their diffusion in some cases and can even lead to NP immobilization in extreme conditions such as tight mesh and adhesive interactions.[5–7]

This is notably the case in ophthalmology. Drugs are often administered into the back of the eye by performing an intravitreal injection.[6,11] This technique often results in the immediate immobilization of the NPs at the injection site.[8] This has been mainly investigated by qualitatively studying the diffusion of polystyrene and lipid NPs. Focusing on the electrostatic interactions between the NPs and the media, several groups showed a clear difference depending on the NP charge.[9–11] A few quantitative studies showed that anionic NPs diffuse up to 1000-fold faster than the cationic ones in the vitreous.[8] For plasmonic NPs, Sauvage et al. showed that 70 nm AuNPs had a diffusion coefficient of 1.9 $\mu m^2\ s^{-1}$ in the vitreous while coated with hyaluronic acid (HA), an anionic polymer largely present in the vitreous. However, they were stuck in the vitreous while coated with PDDAC (poly(diallyldimethylammonium chloride)), a cationic polymer.[12] The impact of the NP size has been mainly of interest to estimate the mesh size of the vitreous rather than a parameter for the diffusion behavior in those applications.[9] Indeed, since vitreous, mucus, and most other biological fluids contain some fiber molecules, such as collagen or fibrin, the mesh size must also be considered to avoid immobilization of the NPs at the injection site.[4,13,14]

In addition to those chemical interactions with biological fluids, the classic Stokes-Einstein relationship (SER) (Equation 1) has restricted applications, making it harder to estimate diffusion coefficients correctly beforehand.

$$D_{SE} = \frac{k_B T}{6\pi\eta_m r_h} \quad (1)$$

I. Largillière, D. Sullivan, M. Meunier
Department of Engineering Physics
Polytechnique Montréal
Montréal, Québec H3C 3A7, Canada
E-mail: michel.meunier@polymtl.ca

The ORCID identification number(s) for the author(s) of this article can be found under https://doi.org/10.1002/smll.202404389

DOI: 10.1002/smll.202404389

In the SER, the diffusion coefficient depends on the temperature T, the macroscopic viscosity η_m, and the hydrodynamic radius of the particle r_h. However, to be accurate, the probe needs to respect the following assumption: the solvent has to be much smaller than the solute. When interested in nanotechnology or biomedical applications, nanoparticles or biological molecules often do not respect this assumption required for the SER, inducing the SER breakdown.

Over the last decades, different techniques have been developed to evaluate the diffusion behavior of various NPs in those conditions. In biological applications, many probes are fluorescent and can be easily detected to estimate their average diffusion. Fluorescence correlation spectroscopy (FCS) is based on fluorescence intensity fluctuations and necessitates a complex system and numerous calculations.[15] Fluorescence recovery after photobleaching (FRAP) relies on the photobleaching properties of the fluorescent label. It has been used since mid-1970s,[16] but the measurements can be quite long for slow diffusing probes.[17,18] It has been adapted for plasmonic NPs that can scatter light, a characteristic used in the scattering recovery after fragmentation (SRAF) technique. Instead of photobleaching, the NPs are fragmented, and their small pieces have a scattering intensity and cross-sections too low to be visible by optical microscopy, but this technique has been shown to underestimate slightly the diffusion coefficient.[12] On the other hand, nanoparticle tracking analyzers (NTA), based on the ultramicroscope principle, allow us to easily get the diffusion coefficient for a single NP or an NP population and other information about the NP colloid sample. However, this type of device can be costly.[19,20]

The objective of this paper is twofold: i) we propose another methodology to precisely determine the diffusion behavior of plasmonic NPs that involves monitoring the scattering of an ensemble of NPs irradiated with light from the side and ii) we introduce a generalized equation to describe the diffusion behavior in viscous environment based on the adapted Huggins model. The first objective is achieved via a cost-efficient side-illumination device developed by our group.[21] This small device can be adapted to any optical microscope and permits an easy and simple observation of individual NP.[21] Here, as a viscous environment model, we studied the diffusion of AuNPs and AgNPs in HA, biopolymer-based solutions with a molecular weight (MW) of 150–300 kDa (low MW) and 750–1000 kDa (high MW), ranging from the order of a mPa·s (water) to a few tens of mPa·s. Gold and silver were chosen as both compositions are widely used for biomedical applications. The size range, from 60 to 200 nm in diameter, was chosen as the limit of detection by optical microscopy for the lower limit and as the usual biggest NP size used in nanobiotechnologies for the upper limit. First, we characterized the diffusion of citrate-capped AuNPs and AgNPs across different viscosities and HA molecular weights, as well as functionalized AuNPs with an HA coating, mPEG (methyl-polyethylene glycol) coating, and antibody-PEG (Ab-PEG) coating. The choice of functionalization was motivated by biomedical applications where biocompatibility (HA, mPEG) and specificity (Ab-PEG) are required. For the second objective, we used the adapted Huggins model developed by Holyst group to describe the NP behavior at this size range.[22] We also discussed the impact of the functionalization on the diffusion behavior of the NPs and the resulting chemical interactions.

2. System and Calculations

2.1. Diffusion Measurement System

The Brownian motion of the NPs were analyzed to determine their diffusion coefficients. First, the colloidal suspensions of NPs were diluted in the media of interest and confined between a glass slide and its coverslip with a spacer of 120–240 µm. The Brownian motion was observed at room temperature using the side-illumination device[21] (**Figure 1a**) with a 60x objective and recorded using a pco.panda 4.2 camera from PCO (Kelheim, Germany), at 25 frames per second (fps), except when precised otherwise. The displacements were tracked and then used to calculate NP diffusion coefficients by using the plugin TrackMate for ImageJ developed by Tinevez et al. (Figure 1b).[23] This system enables the diffusion study of single NPs as well as the whole population of NPs. To ensure that the NPs taken into consideration for the calculations were diffusing onto the plane of focus, some filters were applied to the recording. The plugin for ImageJ selects the NPs according to the size and the intensity of the signal from the NPs. Only circular dots of a specific size (≈9 pixels) and quality threshold (depending on the quality of the recording) were considered. Moreover, the depth of field was determined to be ≈1.2 µm. Considering that the distance between the slide and the coverslip is 120–240 µm, the edge effect can be neglected with this shallow depth of field.

2.2. Method to Measure the Diffusion Coefficient

2.2.1. Diffusion Coefficient Calculation

To obtain the diffusion coefficient from the position of the NPs, the usual mean square displacement (MSD) method was used. The experimental diffusion coefficient D_{exp} is determined by Equation (2).

$$D_{exp} = \frac{MSD}{2\, d_{dim}\, t} = \frac{\left\langle \left(x_t - x_0\right)^2 + \left(y_t - y_0\right)^2 \right\rangle}{4t} = \frac{\left\langle r^2_{MSD} \right\rangle}{4t} \quad (2)$$

The parameters x_t, y_t, x_0, and y_0 are the recorded positions at time t and time 0 respectively, the parameter $d_{dim} = 2$ is the dimension considered during the experiment. The diffusion coefficient was obtained by fitting the average $\langle r^2_{MSD} \rangle$ over hundreds of NPs between the second and the fifth time points as established by Ernst et al.[24] As shown by Coglitore et al., there is no statistically significant difference between a diffusion coefficient determined through a dataset with a frame rate of 28 frames per second (fps), typical for a standard camera, or one with a fps of 500, typical for a high-speed camera.[25] Indeed, the precision brought by the higher fps is counterbalanced by the lower illumination level and thus the loss of details.[24] Diffusion coefficients were calculated for at least 150 NPs per condition with a minimum of 50 frames per NPs and 30 frames for NPs of 60 and 80 nm as their scattering intensity is lower, making them harder to track. Typically after 50 frames, the NPs would have an MSD between 0.25 and 4.3 µm^2 depending on the studied conditions. Further analysis was also performed to check the quality of the recorded data

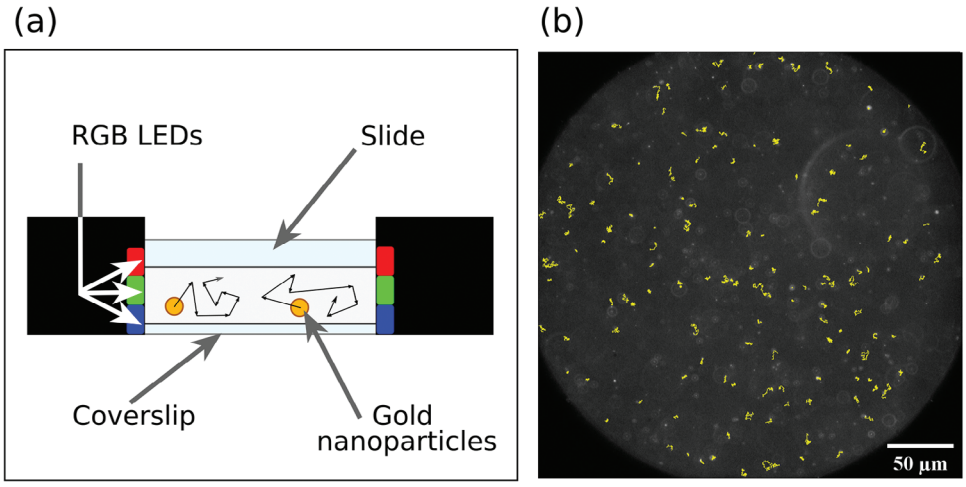

Figure 1. a) Cross-section schematics view of the specially designed red-green-blue (RGB) side-illumination device to monitor the displacement of each AuNP (black arrows) in the solution in the small interspace between the slide and the coverslip (here, it is 120–240 µm). b) A typical example of NPs' trajectories (segments in yellow) was acquired thanks to the Nanotrack plugin for ImageJ open software.[23]

(Figure S2, Supporting Information). The displacements in both directions, x, and y, were compared to an expected normal distribution, and we confirmed the narrow distribution of the diffusion coefficient of each NP under the same experimental conditions.

3. Results

Figures 2, 3 and 4 give the experimental diffusion coefficients D_{exp} as a function of the hydrodynamic radius r_h for AuNPs, AgNPs both coated with citrate and AuNPs coated with various coatings respectively. The different conditions studied have been summarized in **Table 1**.

As shown in Figure 2, the citrate-AuNPs diffusion greatly depends on the macroscopic viscosity η_m and the NP hydrodynamic radius r_h. However, as presented in **Tables 2** and 3, the diffusion coefficient D_{exp} is higher than expected by the SER in the HA solutions and lower for the water as obtained by using Equation (1) with the macroscopic viscosity η_m. This behavior in water was expected and already described by Coglitore et al. for polystyrene NPs and the one in HA medium by Unni et al. for cobalt ferrite NPs.[7,25] On average in

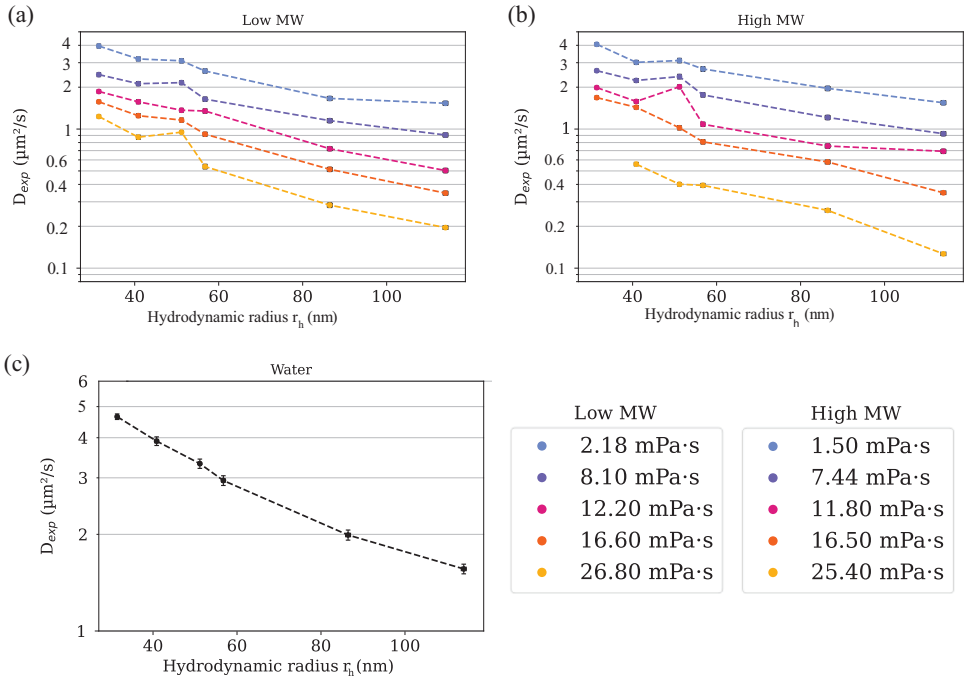

Figure 2. Diffusion coefficients D_{exp} for AuNPs coated with citrate as a function of the hydrodynamic radius r_h for various macroscopic viscosity η_m a) in HA solutions of low MW (150–300 kDa), b) in HA solutions of high MW (750–1000 kDa), and c) in water. The dotted lines are to guide the eyes.

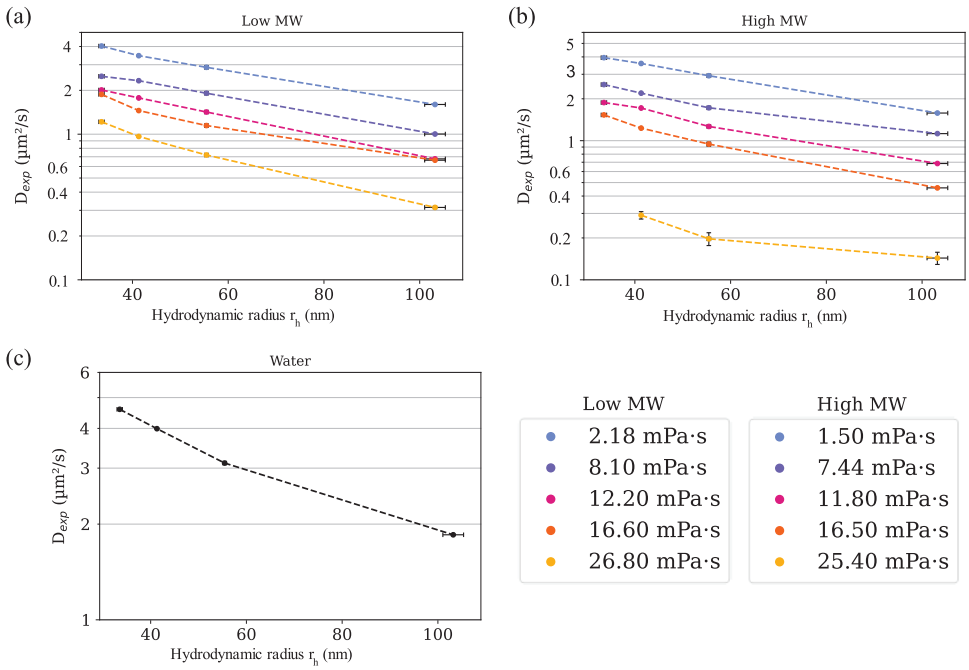

Figure 3. Diffusion coefficients D_{exp} for AgNPs coated with citrate as a function of the hydrodynamic radius r_h for various macroscopic viscosity η_m a) in HA solutions of low MW (150–300 kDa), b) in HA solutions of high MW (750–1000 kDa), and c) in water. The dotted lines are to guide the eyes.

water, the citrate-AuNPs were diffusing 21% lower than expected by the SER. Concerning the HA solutions, for the low MW above 8 mPa·s, the NPs diffuse between 3.5 and 4.5 faster than expected by the SER. For the high MW, the behavior is slightly different. The ratio increases with the viscosity up to 11.8 mPa·s reaching 4.0 and then decreases again to 2.43 at 25.40 mPa·s.

Then, we checked if the citrate-AgNPs (**Figure 3**) had the same behavior as the AuNPs or if the breakdown of the SER was dependent on the composition of the particles. As shown in Tables 1

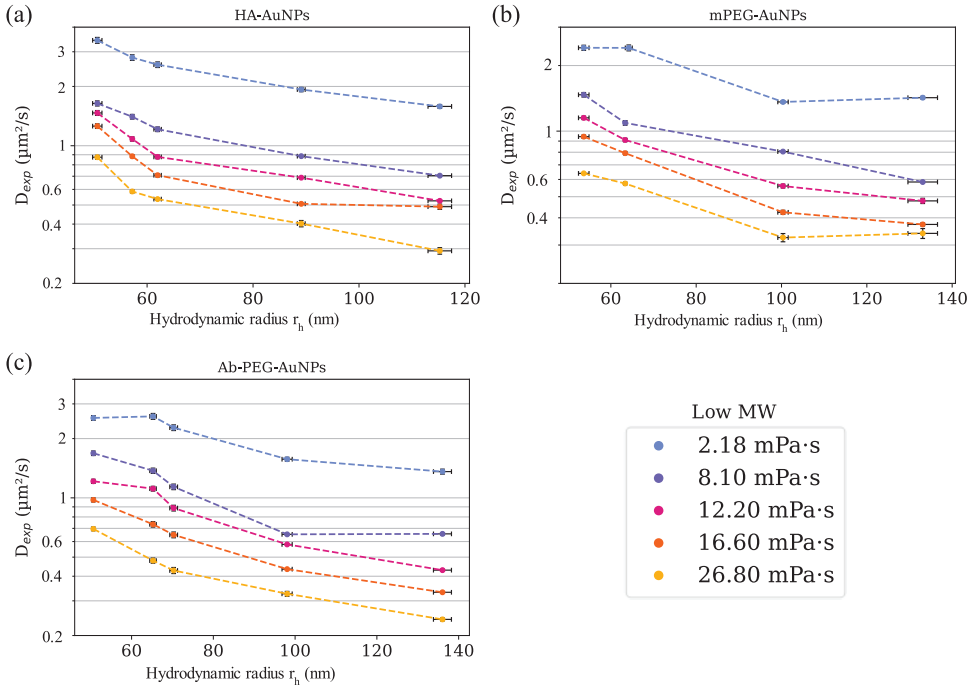

Figure 4. Diffusion coefficients D_{exp} for AuNPs coated with a) HA coating, b) mPEG coating, and c) Ab-PEG coating as a function of the hydrodynamic radius r_h for various macroscopic viscosity η_m in HA solutions of low MW (150–300 kDa). The dotted lines are to guide the eyes.

Table 1. Summary of the parameters studied.

Parameters	Range
NP composition	Au, Ag
NP hydrodynamic radius	30–135 nm
NP coating	Citrate, mPEG, PEG-Ab, HA
Dispersion medium	$PEG_{150\text{-}300\ kDa}$, $PEG_{750\text{-}1000kDa}$
Macroscopic viscosity	1–30 mPa·s

and 2, for the viscosity of 16.5 mPa·s and lower, there is no significant difference between the two compositions. However, for higher viscosity, AgNPs diffuse more slowly than AuNPs for the high MW, with a ratio of 1.49 against 2.43 at 25.40 mPa·s and faster for the low MW, with a ratio of 4.79 against 4.18 at 26.80 mPa·s.

Finally, as AuNPs are usually used with different coatings for biomedical applications, we investigated the impact of the functionalization on diffusion by comparing the citrate coating with an HA coating, a mPEG functionalization, and an Ab-PEG bioconjugation (Figure 4). As presented in Table 3, it is interesting to notice that the AuNPs with citrate and with HA are the ones with the highest diffusion coefficients. AuNPs coated with HA and citrate have similar behavior, ± 16% ratio difference for each condition with an average of 2%. AuNPs coated with mPEG and PEG-Ab have a similar behavior, ± 9% ratio difference for each condition with an average of 1.3%. Lastly, the HA-AuNPs have the closest behavior to the ones of citrate-AuNPs (a difference of 2% on average), followed by the bioconjugated ones (a difference of 3.8% on average) and mPEG ones (a difference of 4.85 on average). The complete data can be found in the Excel file of the supplementary information and the characterization of the NPs in Table S2 and Figure S3 (Supporting Information).

4. Discussion

To explain the difference between the SER prediction and the experimental results, we can consider the hypothesis behind the SER. As explained by Capalezzo et al., the frictional resistance and the average viscosity are proportional only if the velocity of the probe is smaller than the average atomic motion of the solvent. This is not the case anymore if the thermal velocities are similar, that is to say if the sizes of the NPs and the solvent are comparable.[26] To address the behavior of the probes in those situations, the fractional SER has been developed introducing a weaker dependence in $(1/\eta)$. With this approach, Coglitore et al. have highlighted an SER breakdown for NPs below 150–300 nm with a dependence of D in η^{-p} instead of η^{-1}[25] with p being 0.84. It has been used when the probe size is similar to the solvent size,[25,27,28] However, if this strategy enables the description of the diffusion, it is fully empirical, and cannot be generalized for further conditions and neglects the size impact.

Table 2. Ratio between the experimental diffusion coefficient D_{exp} and the D_{SE} (Equation (1)) for AuNPs and AgNPs in low MW (150–300 kDa) viscous solutions.

Condition		Ratio D_{exp}/D_{SE}	
		Citrate-AuNPs	Citrate-AgNPs
Water		0.79	0.82
High	1.50 mPa·s	1.06	1.06
	7.44 mPa·s	3.51	3.36
	11.80 mPa·s	4.00	3.79
	16.50 mPa·s	3.85	3.89
	25.40 mPa·s	2.43	1.49

An alternative approach is to introduce an effective or nano-viscosity η_{eff} to replace the macroscopic viscosity η_m into the SER. Equation (1) is now modified as Equation (3).

$$D = \frac{k_B T}{6\pi \eta_{eff} r_h} \tag{3}$$

Some models rely on hydrodynamics such as the Huggins model, $\eta_{eff} = \eta_s\ exp(k\frac{r_h}{E})$, further adapted by De Smedt et al. et re-used by Unni et al.,[7,17,29] This model depends on the solvent viscosity η_s, the hydrodynamic radius of the probe r_h, and the correlation length E of the polymer and k being a fitting parameter. All the characteristic lengths of the polymers that include the correlation length can be found in Table S1 (Supporting Information), and here, the solvent viscosity is the viscosity of water at 19 °C with the tabulated value of 1.027 mPa·s. However, this model has been developed as an alternative to the SER when the probe size does not respect this hypothesis anymore and is not generalizable at all scales. As the Huggins model is limited due to its approximation, the estimations were not optimal and led to errors superior to 50% between the experimental effective viscosity and the one estimated by the model as shown in Tables S5,S6 and Figure S4 (Supporting Information). Cai et al.[30] also described the diffusion behavior depending on the probe scale compared to the polymer and highlighted three different regimes (small, intermediate, and large probes). They developed a model for each regime thanks to approximations valid in each condition. However, there is not only one equation to describe diffusion behavior at all scales.

To obtain a better description of D_{exp} and η_{eff}, we investigated a slightly more complex model developed for polymer-based systems by the Holyst group, that developed an empirical equation to fit the experimental diffusion. This model is referred below as the adapted Huggins model. Indeed, they introduced an effective radius in the Huggins model as shown in Equation (4) that enables the description of the diffusion behavior for all sizes of probes,[22,31–33] By introducing an equation valid at all scales, they have bypassed the previous issues.

$$\eta_{eff} = \eta_s \times \exp\left(k\left(\frac{R_{eff}}{E}\right)^a\right) \tag{4}$$

In this equation, k is a system-dependent parameter related to the energy and a is a scaling parameter.[34] The effective radius R_{eff} (Equation (5)) takes into account the relationship between the hydrodynamic radius of the probe r_h and the hydrodynamic radius of the polymer R_h.

$$R_{eff}^{-2} = r_h^{-2} + R_h^{-2} \tag{5}$$

Table 3. Ratio between the experimental diffusion coefficient D_{exp} and the D_{SE} (Equation (1)) for AuNPs and AgNPs having different coatings in high MW (750–1000 kDa) viscous solutions.

Condition	Ratio D_{exp}/D_{SE}				
	Citrate-AuNP	HA-AuNP	mPEG-AuNP	Ab-PEG-AuNP	Citrate-AgNP
2.18 mPa·s	1.49	1.73	1.51	1.62	1.54
8.10 mPa·s	3.60	3.02	3.01	3.09	3.69
12.20 mPa·s	3.70	3.56	3.34	3.56	4.13
16.60 mPa·s	3.82	4.03	3.62	3.58	4.94
26.80 mPa·s	4.18	4.52	4.43	4.04	4.79

Moreover, this adapted model correctly considers the two limits, for small or large probes where the effective viscosity should be the solvent one and the macroscopic one respectively. They tested their model for probes ≈1–10 nm. After their first empirical equation development, the Holyst group broadened its applications from simple polymer solutions to polymer mixtures or polyelectrolyte solutions.[22,32,33] They also highlighted the existence of different regimes depending on the polymer concentration: dilute, semi-dilute, and concentrated. It impacts at least the value of the parameter a from Equation (4).[31] By putting D of Equation (3) equals to D_{exp}, we determined η_{eff} and were able to use the previous model in the following discussion.

The accuracy of the model with the experimental data is shown in **Figure 5** and the estimated k and a parameters and the root mean square error (RMSE) are given in **Tables 4** and **5**. With this adapted Huggin's model, the effective viscosity is better represented and the RMSE on the effective viscosity drops ≈12.9% on average for the low MW and 31.6% for the high MW. The parameter k is ≈2–2.5 for both MW. On the other hand, the parameter a is equal to 0.69–0.77 for the high MW and decreases to 0.47–0.58 for the low MW. We can notice that the parameter estimation depends on the coating.

However, to ensure that the effective radius R_{eff} depends on the surface of the system probe-polymer, and not the dimension or the volume, as a function of the polymer regime of the solution, we have tested this hypothesis using R^{-1} and R^{-3} in the supplementary information resulting in not much better fit (Figure S5 and Table S7, Supporting Information).

As shown in Table 5, the coatings have an impact on the k and a parameters for the adapted Huggins model. Based on the suggestion by Giorgi et al.[35] that the chemical interactions at the nanoscale can influence the diffusion behavior, we proposed that the coating affects these interactions as indicated by the change in zeta potential.

Considering the limit for large probes in the adapted Huggins models, the effective viscosity limit η_{lim} should be equal to the macroscopic one η_m (Equation (6)).

$$\eta_{lim} = \lim_{r_h \to +\infty} \eta_{eff} = \eta_s \, exp\left(k\left(\frac{R_h}{E}\right)^a\right) \quad (6)$$

As shown in **Figure 6a**, the viscosity η_{lim} for citrate-AuNPs is largely inferior to the macroscopic viscosity η_m and the gap increases with the concentration: 30% lower at low concentration and 70% lower at high concentration. As citrate is negatively charged, it induces repulsive electrostatic interactions between the NPs and the HA strands. It might explain the decrease in effective viscosity felt by the NPs and thus η_{lim}. Now, broadening the analysis to the other coatings, one can notice that their viscosity η_{lim} is similar when compared to the macroscopic viscosity η_m (Figure 6). However, Figure 6b highlights that the η_{lim} is higher for mPEG and HA than for citrate and Ab-PEG at high concentration (maximum difference of 1.27 mPa·s) but is negligible at low concentration (maximum difference of 0.16 mPa·s). This is confirmed with the adapted Huggins model where both parameters, a and k, are decreasing from citrate to Ab-PEG, HA, and finally mPEG (Table 5). This trend seems to be more important at high concentration whereas more interactions between the NPs and the HA strands can happen, and proportional to the zeta potential, and thus the NP charge at the exception of Ab-PEG-NPs. This difference may be due to other interactions that might take place such as Van der Waals or hydrophobic repulsions. To explain the behavior at high concentration, we can look into the mesh constituted by HA. The mesh becomes tighter with the concentration increasing and thus, the correlation length decreasing (Table S1, Supporting Information). Then, it is harder for the NPs to deform the mesh to pass through the pores as the NP charge increases, leading to an increase in the repulsive interactions, and therefore the deformations need to be more important for the NP to flow through the mesh.[36]

5. Conclusion

In summary, it is important to estimate and model the diffusion of plasmonic NPs for nanotechnology applications. The key message is the validation of the Huggins adapted model for NPs from 30–135 nm (hydrodynamic radius) and the non negligible impact of the coating for the NP diffusion. The side-illumination device, easily adapted to any optical microscope, allowed to follow the Brownian motion of plasmonics nanoparticles of radius larger than 30 nm, thus having sufficient scattering cross-section. With the large range of investigated conditions of viscosity from 1.0 to 26.8 mPa·s and NPs radius from 30 to 135 nm, this study enabled the characterization of NP diffusion behavior in the range from 0.13 to 4.65 $\mu m^2\ s^{-1}$. Measured diffusion coefficients are found to be up to 4–5 times greater than expected by the SER using the macroscopic viscosity of the solution. We validated that the adapted Huggins equation (Equation (4) and with R_{eff} defined as in Equation (5)) is a good model for estimating the effective viscosity η_{eff} for NPs with a size of the same order of magnitude as

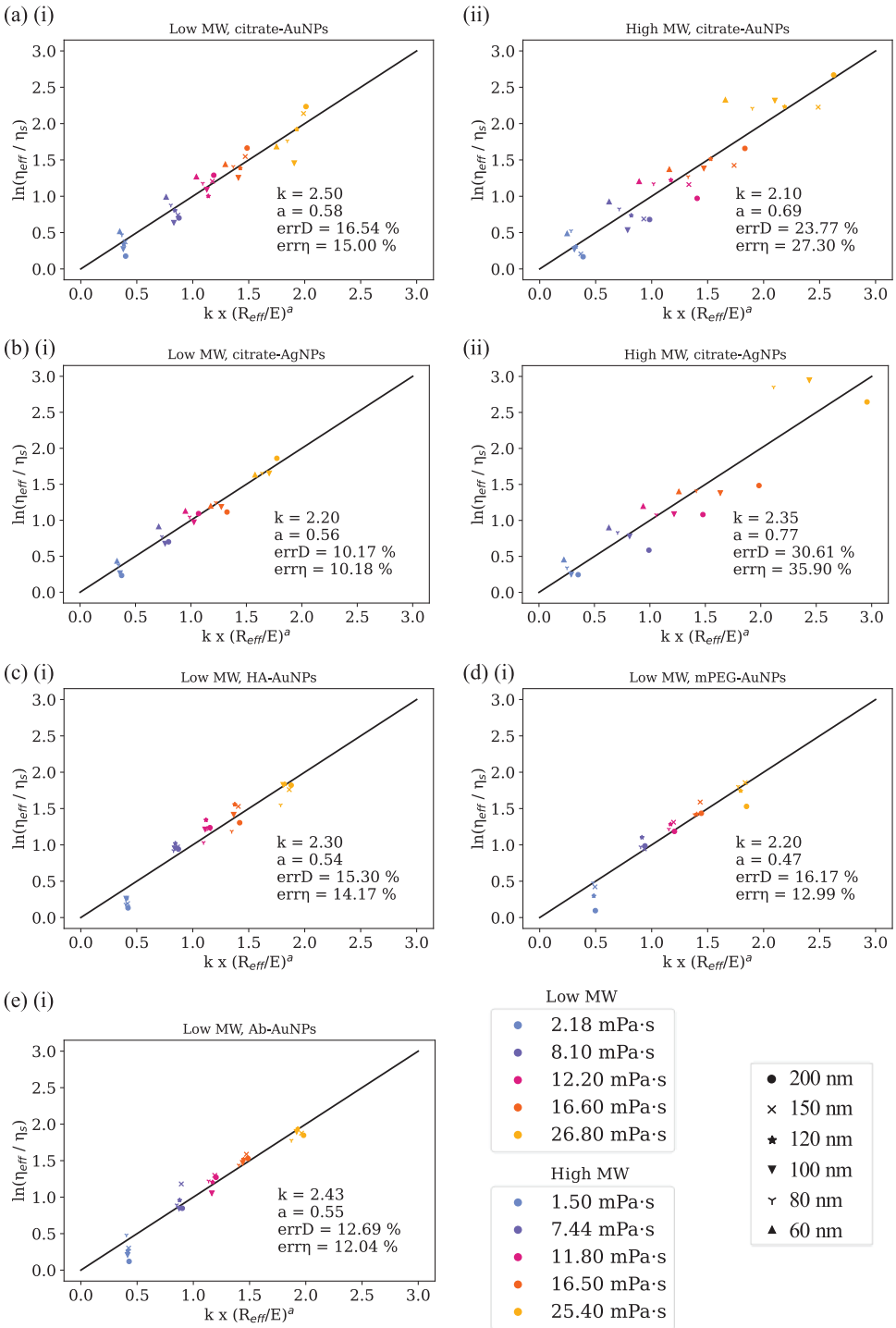

Figure 5. Natural logarithm of the viscosity ratio as a function of k $(R_{eff}/E)^a$ as given by Equation (4) for all experimental data a) for citrate-AuNPs, b) for citrate-AgNPs c) for HA-AuNPs, d) for mPEG-AuNPs, and e) for Ab-PEG-AuNPs. Results (i) in the low MW and (ii) in the high MW HA solutions. The value of R_{eff} can be found in Tables S3 and S4 (Supporting Information). For each condition, the best values of k and a with the corresponding errors on D_{exp} and h_{eff} are given.

Table 4. Estimations of the parameters *k* and *a* for the adapted Huggins model in high MW HA solutions and RMSE in percentage. Measured zeta potentials ζ are also given. The measurements are done in MilliQ water with a pH of 7 and a resistivity of 18.2 MΩ·cm and the Huckel approximation of the Henry equation was used.

Conditions	k	a	Mean ζ-potential [mV]	RMSE on D	RMSE on η
Citrate-AuNP	2.10	0.69	−41.9	23.8	27.3
Citrate-AgNP	2.35	0.77	−43.7	30.6	35.9

Table 5. Estimations of the parameters *k* and *a* for the adapted Huggins model in low MW HA solutions and RMSE in percentage. Measured zeta potentials ζ are also given. The measurements are done in MilliQ water with a pH of 7 and a resistivity of 18.2 MΩ·cm and the Huckel approximation of the Henry equation was used.

Conditions	k	a	Mean ζ-potential (mV)	RMSE on D	RMSE on η
Citrate-AuNP	2.50	0.58	−41.9	16.5	15
Ab-PEG-AuNP	2.43	0.55	−20.7	12.7	12.0
HA-AuNP	2.30	0.54	−32.9	15.3	14.2
mPEG-AuNP	2.20	0.47	−25.8	16.2	13.0
Citrate-AgNP	2.20	0.56	−43.7	10.2	10.2

the polymer. Indeed, the parameters k and a describing η_{eff} are obtained for all conditions describing the measured diffusion coefficient with the RMSE as good as below 16.5% for any conditions tested in the HA solutions of 150–300 kDa. Thus combining Equations (3–5), the diffusion coefficient is given by:

$$D = \frac{k_B T}{6\pi r_h \eta_s \cdot \exp\left(k\left(\frac{\left(r_h^{-2}+R_h^{-2}\right)^{-1/2}}{E}\right)^a\right)} \quad (7)$$

where the hydrodynamic radius of the plasmonic NPs is r_h and all characteristics of the polymeric solutions (η_s, R_h and E) have to be used. The parameter a is a scaling parameter of values 0.47–0.77 for the studied conditions and k is a system-dependent parameter related to the energy with values 2.10–2.50.

In addition, as shown by the results for the different functionalizations, the chemical interactions between the probes and the polymer influence the estimation of the model parameters and can not be neglected. This outcome highlights the need to further improve the model to include the influence of chemical interactions, probably the electrostatic repulsions or attractions, and the dependence on the charges of the polymer and the probes. In future studies, the effect of temperature may be considered as well as to better understand the effect of chemical interactions, a larger number of coatings could be investigated and may lead to the implementation of the chemical interaction impact into the model.

6. Experimental Section

Materials: Citrate-capped gold nanoparticles with nominal diameters of 60 nm (polydispersity index (PDI) of 9.4%), 80 nm (PDI of 10.9%), and 100 nm (PDI of 6.7%) were purchased from NanoComposix (San Diego, CA, USA). Citrate-capped gold nanoparticles with a nominal diameter of 150 nm (PDI of 3%) and 200 nm (PDI of 3%) were purchased from Nanopartz (Loveland, CO, USA). Citrate-capped gold nanoparticles with nominal diameters of 120 nm were prepared by the Turkevich method.[37] To prepare the viscous solution, hyaluronic acid (HA) from Bulk Supplements (Henderson, NV, USA) was used of 150–300 kDa (measured by Western Blot, data not shown) and HA from Sigma–Aldrich (Saint-Louis, MO, USA) of 750–1000 kDa. To functionalize the NPs, HA of 15–30 kDa from Sigma–Aldrich (Saint-Louis, MO, USA), mPEG-SH of 5 kDa, and HS-PEG-COOH of 1 kDa and 5 kDa from Nanocs (New-York, NY, USA) and anti-CD44 antibodies (reference MA4400), EDC and sulfo-NHS from ThermoFisher (Waltham, MA, USA) were used.

Viscous Environnements: *Fabrication of the viscous liquids*: The different viscous solutions were obtained by dissolving 10 mg of HA of different molecular weights in 10 mL of distilled water and by cascade dilution for the lower concentrations (0.5, 0.3, 0.15, and 0.025 mg mL^{-1}).

Rheology test: The standard viscosities of the HA solutions were measured using a Physica MCR 501 rheometer from Anton Paar (Graz, Austria). The measurements were carried out in rotation with a shear rate evolving from 1000 to 0.01 s^{-1} at a fixed temperature of 22 °C. The results are shown in Figure S1 (Supporting Information).

Coatings of the NPs: *Coating AuNPs with Hyaluronic Acid*: Before incubating the AuNPs with HA, the NPs were diluted to 2 × 10^9 NPs mL^{-1}. Next, 10 µL of HA at 3 mg mL^{-1} was added to 500 µL of AuNPs and kept overnight at 4 °C. The AuNPs were centrifugated for 5 min at 2000 g for NPs below 100 nm and at 1200 g for NPs of 100 nm and above and resuspended in water.

PEGylation of AuNPs: The AuNPs were sonicated for a few minutes before use. Respectively, 30 µL of mPEG-SH (5 kDa) dissolved in dH_2O at 10 mg mL^{-1} after TCEP treatment were added to 1 mL of AuNPs at

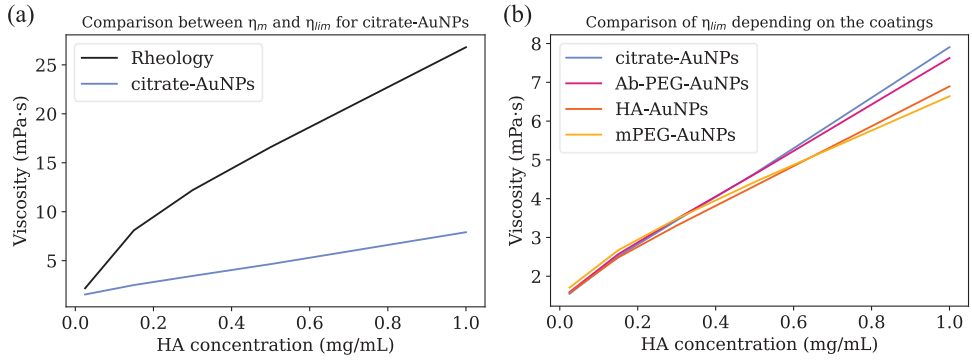

Figure 6. a) Macroscopic viscosity (rheology) and effective viscosity limit η_{lim} from the citrate-AuNPs diffusion model as a function of the low MW HA concentration. b) Effective viscosity limit η_{lim} from the AuNPs diffusion model for the different coating studied (citrate, Ab-PEG, mPEG, and HA) as a function of the low MW HA concentration.

stock concentration. The solutions were briefly vortexed and kept at 4 °C overnight. The NPs were centrifugated twice for 5 min at 2000 g for NPs below 100 nm and at 1200 g for NPs of 100 nm and above and resuspended in water.

Functionalization of AuNPs with antibody: The AuNPs were sonicated for a few minutes before use. Then, 30 µL of HS-PEG-COOH (5 kDa) dissolved in dH_20 at 10 mg mL^{-1} after TCEP treatment were added to 1 mL of AuNPs of 100 nm or above, or 30 µL of HS-PEG-COOH (1 kDa) dissolved in dH_20 at 10 mg mL^{-1} were added to 1 mL of AuNPs below 100 nm. The solutions were briefly vortexed and kept at 4 °C overnight. The NPs were centrifugated twice for 5 min at 2000 g for NPs below 100 nm and at 1200 g for NPs of 100 nm and then resuspended in dH_2O. Next, 0.7 µL of EDC at 10 mg mL^{-1} and 1.3 µL of sulfo-NHS at 10 mg mL^{-1} were added to the AuNPs. The solutions were vortexed for homogenization and incubated for 30 min on a rotator at room temperature. The NPs were centrifugated for 5 min at 2000 g for NPs below 100 nm and at 1200 g for NPs of 100 nm and above and then resuspended in PBS-Tween20 (0.1%). Then, 1 µg of antibodies were added to the solutions and kept for 1 h on a rotator. Finally, the solutions were centrifuged (thrice for 5 min at 2000 g for NPs below 100 nm and at 1200 g for NPs of 100 nm and above) and resuspended in water.

Supporting Information

Supporting Information is available from the Wiley Online Library or from the author.

Acknowledgements

This work was financed by the Natural Sciences and Engineering Research Council of Canada (NSERC). The authors acknowledge interesting discussions with Scott G. Harroun and Cécile Darviot, the help of Sergiy Patskovsky for the side-illumination device, the technical help of Yves Drolet, and the help with the rheology measurements from Matthieu Gauthier.

Conflict of Interest

The authors declare no conflict of interest.

Data Availability Statement

The data that support the findings of this study are available in the supplementary material of this article.

Keywords

adapted Huggins model, diffusion, effective viscosity, gold nanoparticles, silver nanoparticles, viscous environment

Received: May 30, 2024
Revised: August 6, 2024
Published online:

[1] L. Wang, M. H. Kafshgari, M. Meunier, *Adv. Funct. Mater.* **2020**, *30*, 2005400.
[2] E. Boisselier, D. Astruc, *Chem. Soc. Rev.* **2009**, *38*, 1759.
[3] G. R. Tortella, O. Rubilar, N. Durán, M. C. Diez, M. Martínez, J. Parada, A. B. Seabra, *J. Hazard. Mater.* **2020**, *390*, 121974.
[4] T. Stylianopoulos, M.-Z. Poh, N. Insin, M. G. Bawendi, D. Fukumura, L. L. Munn, R. K. Jain, *Biophys. J.* **2010**, *99*, 1342.
[5] S. K. Lai, D. E. O'Hanlon, S. Harrold, S. T. Man, Y.-Y. Wang, R. Cone, J. Hanes, *Proc. Natl. Acad. Sci., USA* **2007**, *104*, 1482.
[6] B. T. Käsdorf, F. Arends, O. Lieleg, *Biophys. J.* **2015**, *109*, 2171.
[7] M. Unni, S. Savliwala, B. D. Partain, L. Maldonado-Camargo, Q. Zhang, S. Narayanan, E. M. Dufresne, J. Ilavsky, P. Grybos, A. Koziol, P. Maj, R. Szczygiel, K. D. Allen, C. M. Rinaldi-Ramos, *Sci. Adv.* **2021**, *7*, eabf8467.
[8] Q. Xu, N. J. Boylan, J. S. Suk, Y.-Y. Wang, E. A. Nance, J.-C. Yang, P. J. McDonnell, R. A. Cone, E. J. Duh, J. Hanes, *J. Controlled Release.* **2013**, *167*, 76.
[9] E. M. del Amo, A.-K. Rimpelä, E. Heikkinen, O. K. Kari, E. Ramsay, T. Lajunen, M. Schmitt, L. Pelkonen, M. Bhattacharya, D. Richardson, A. Subrizi, T. Turunen, M. Reinisalo, J. Itkonen, E. Toropainen, M. Casteleijn, H. Kidron, M. Antopolsky, K.-S. Vellonen, M. Ruponen, A. Urtti, *Prog. Retinal Eye Res.* **2017**, *57*, 134.
[10] S. Tavakoli, O. K. Kari, T. Turunen, T. Lajunen, M. Schmitt, J. Lehtinen, F. Tasaka, P. Parkkila, J. Ndika, T. Viitala, H. Alenius, A. Urtti, A. Subrizi, *Mol. Pharmaceutics.* **2021**, *18*, 699.
[11] X. Huang, Y. Chau, *Exp. Eye Res.* **2019**, *186*, 107711.
[12] F. Sauvage, J. C. Fraire, K. Remaut, J. Sebag, K. Peynshaert, M. Harrington, F. J. Van de Velde, R. Xiong, M.-J. Tassignon, T. Brans, K. Braeckmans, S. C. De Smedt, *ACS Nano.* **2019**, *13*, 8401.
[13] V. Gowd, A. Ahmad, M. Tarique, M. Suhail, T. A. Zughaibi, S. Tabrez, R. Khan, *Semin. Cancer Biol.* **2022**, *86*, 624.
[14] B. S. Schuster, J. S. Suk, G. F. Woodworth, J. Hanes, *Biomaterials* **2013**, *34*, 3439.
[15] L. Yu, Y. Lei, Y. Ma, M. Liu, J. Zheng, D. Dan, P. Gao, *Front. Phys.* **2021**, *9*, 644450.
[16] N. Lorén, J. Hagman, J. K. Jonasson, H. Deschout, D. Bernin, F. Cella-Zanacchi, A. Diaspro, J. G. McNally, M. Ameloot, N. Smisdom, M. Nydén, A.-M. Hermansson, M. Rudemo, K. Braeckmans, *Q Rev. Biophys.* **2015**, *48*, 323.
[17] S. C. De Smedt, A. Lauwers, J. Demeester, Y. Engelborghs, G. De Mey, M. Du, *Macromolecules.* **1994**, *27*, 141.
[18] E. Evoy, A. M. Maclean, G. Rovelli, Y. Li, A. P. Tsimpidi, V. A. Karydis, S. Kamal, J. Lelieveld, M. Shiraiwa, J. P. Reid, A. K. Bertram, *Atmos. Chem. Phys.* **2019**, *19*, 10073.
[19] T. M. M. Ways, S. K. Filippov, S. Maji, M. Glassner, M. Ceglowski, R. Hoogenboom, S. King, W. M. Lau, V. V. Khutoryanskiy, *J. Colloid Interface Sci.* **2022**, *626*, 251.
[20] E. A. Mun, C. Hannell, S. E. Rogers, P. Hole, A. C. Williams, V. V. Khutoryanskiy, *Langmuir.* **2014**, *30*, 308.
[21] M. Qi, C. Darviot, S. Patskovsky, M. Meunier, *Analyst.* **2019**, *144*, 1303.
[22] K. Sozanski, A. Wisniewska, T. Kalwarczyk, A. Sznajder, R. Holyst, *PLoS One.* **2016**, *11*, 0161409.
[23] J.-Y. Tinevez, N. Perry, J. Schindelin, G. M. Hoopes, G. D. Reynolds, E. Laplantine, S. Y. Bednarek, S. L. Shorte, K. W. Eliceiri, *Methods.* **2017**, *115*, 80.
[24] D. Ernst, J. Köhler, *Phys. Chem. Chem. Phys.* **2013**, *15*, 845.
[25] D. Coglitore, S. P. Edwardson, P. Macko, E. A. Patterson, M. Whelan, *R. Soc. Open Sci.* **2017**, *4*, 170507.
[26] M. Cappelezzo, C. A. Capellari, S. H. Pezzin, L. A. F. Coelho, *J. Chem. Phys.* **2007**, *126*, 224516.
[27] L. Xu, F. Mallamace, Z. Yan, F. W. Starr, S. V. Buldyrev, H. E. Stanley, *Nat. Phys.* **2009**, *5*, 565.
[28] K. R. Harris, *J. Chem. Phys.* **2009**, *131*, 054503.
[29] M. L. Huggins, *J. Am. Chem. Soc.* **1942**, *64*, 2716.
[30] L.-H. Cai, S. Panyukov, M. Rubinstein, *Macromolecules.* **2011**, *44*, 7853.
[31] A. Agasty, A. Wisniewska, T. Kalwarczyk, K. Koynov, R. Holyst, *ACS Appl. Polym. Mater.* **2021**, *3*, 2813.

[32] A. Wisniewska, K. Sozanski, T. Kalwarczyk, K. Kedra-Krolik, R. Holyst, *Macromolecules.* **2017**, *50*, 4555.
[33] G. Bubak, K. Kwapiszewska, T. Kalwarczyk, K. Bielec, T. Andryszewski, M. Iwan, S. Bubak, R. Holyst, *J. Phys. Chem. Lett.* **2021**, *12*, 294.
[34] J. Michalski, T. Kalwarczyk, K. Kwapiszewska, J. Enderlein, A. Poniewierski, A. Karpinska, K. Kucharska, R. Holyst, *Soft Matter.* **2024**, *20*, 5810.
[35] F. Giorgi, D. Coglitore, J. M. Curran, D. Gilliland, P. Macko, M. Whelan, A. Worth, E. A. Patterson, *Sci. Rep.* **2019**, *9*, 12689.
[36] T. Sakai, M. Kurakazu, Y. Akagi, M. Shibayama, U. Chung, *Soft Matter.* **2012**, *8*, 2730.
[37] J. Turkevich, P. C. Stevenson, J. Hillier, *Discuss. Faraday Soc.* **1951**, *11*, 55.